AGU PUBLICATIONS

JGR

Journal of Geophysical Research: Atmospheres

RESEARCH ARTICLE
10.1002/2016JD025597

Key Points:
- 1.Noah-MP-Crop is able to capture the seasonal and annual variability of crop-specific LAI and biomass.
- 2.The improved estimation of LAI in Noah-MP-Crop led to more accurate surface sensible and latent heat flux simulations.
- 3.It is necessary to incorporate field management information in Cropland related simulations.

Supporting Information:
- Figure S1

Correspondence to:
D. Niyogi,
dniyogi@purdue.edu

Citation:
Liu, X., F. Chen, M. Barlage, G. Zhou, and D. Niyogi (2016), Noah-MP-Crop: Introducing dynamic crop growth in the Noah-MP land surface model, *J. Geophys. Res. Atmos.*, *121*, 13,953–13,972, doi:10.1002/2016JD025597.

Received 6 JUL 2016
Accepted 28 OCT 2016
Accepted article online 2 NOV 2016
Published online 14 DEC 2016

Noah-MP-Crop: Introducing dynamic crop growth in the Noah-MP land surface model

Xing Liu[1], Fei Chen[2], Michael Barlage[2], Guangsheng Zhou[3], and Dev Niyogi[1,4]

[1]Department of Agronomy, Purdue University, West Lafayette, Indiana, USA, [2]National Center for Atmospheric Research, Boulder, Colorado, USA, [3]Chinese Academy of Meteorological Science, Beijing, China, [4]Department of Earth, Atmospheric, and Planetary Sciences, Purdue University, West Lafayette, Indiana, USA

Abstract Croplands are important in land-atmosphere interactions and in the modification of local and regional weather and climate; however, they are poorly represented in the current version of the coupled Weather Research and Forecasting/Noah with multiparameterization (Noah-MP) land surface modeling system. This study introduced dynamic corn (*Zea mays*) and soybean (*Glycine max*) growth simulations and field management (e.g., planting date) into Noah-MP and evaluated the enhanced model (Noah-MP-Crop) at field scales using crop biomass data sets, surface heat fluxes, and soil moisture observations. Compared to the generic dynamic vegetation and prescribed-leaf area index (LAI)-driven methods in Noah-MP, the Noah-MP-Crop showed improved performance in simulating leaf area index (LAI) and crop biomass. This model is able to capture the seasonal and annual variability of LAI and to differentiate corn and soybean in peak values of LAI as well as the length of growing seasons. Improved simulations of crop phenology in Noah-MP-Crop led to better surface heat flux simulations, especially in the early period of growing season where current Noah-MP significantly overestimated LAI. The addition of crop yields as model outputs expand the application of Noah-MP-Crop to regional agriculture studies. There are limitations in the use of current growing degree days (GDD) criteria to predict growth stages, and it is necessary to develop a new method that combines GDD with other environmental factors, to more accurately define crop growth stages. The capability introduced in Noah-MP allows further crop-related studies and development.

1. Introduction

This study aims to improve the representation of cropland-atmosphere interactions in the Noah with multiparameterization (Noah-MP) [*Niu et al.,* 2011] land surface model with the ultimate goal of coupling it with the mesoscale Weather Research and Forecasting (WRF) numerical weather prediction and regional climate model. Croplands cover 12.6% of the global land and 19.5% of the continental United States. The efficiency with which crops transfer water vapor from the crop root zones to the atmosphere heavily depends on seasonal variations of crop phenology. Crops have a detectable influence on regional distributions of atmospheric water vapor and temperature and can affect convective triggering by modifying mesoscale boundaries [*Raddatz*, 1998; *Changnon et al.,* 2003; *Levis et al.,* 2012]. Therefore, croplands can significantly influence land-atmosphere coupling, surface exchanges of heat, water vapor, and momentum, which in turn can impact boundary layer growth and mesoscale convergence/convection [*Freedman et al.,* 2001; *McPherson et al.,* 2004].

Despite considerable improvements in land surface models (LSM) [e.g., *Niyogi et al.,* 2009; *Niu et al.,* 2011; *Barlage et al.,* 2015], the representation of dynamic cropland processes within the operational WRF model has been absent. Global climate models (GCMs), on the other hand, have attempted to include two-way crop-atmosphere interactions, which improved model performance [*Tsvetsinskaya et al.,* 2001; *Osborne et al.*, 2009; *Levis et al.,* 2012]. Recently, *Lu et al.* [2015] and *Harding et al.* [2015] used coupled WRF/Community Land Model (CLM)-Crop to study the impacts of dynamic crop growth on surface fluxes and irrigation; they concluded that dynamic crop growth should be included in coupled land surface-atmospheric models. *Xu and Hoffman*, [2015] evaluated the Couple Model Intercomparison Project Phase 5 simulations over cropland flux sites; they also suggested incorporating process-based crop models in coupled land surface-atmospheric models.

The Noah with multiparameterization options (Noah-MP) LSM is a new-generation community land model, using multiple options for key land-atmosphere interaction processes to represent seasonal and annual

cycles of snow, hydrology, and vegetation [*Niu et al.,* 2011; *Yang et al.,* 2011]. It has been implemented in the WRF model [*Barlage et al.,* 2015] for real-time operations. The Noah-MP model was evaluated using in situ and satellite data [*Niu et al.,* 2011; *Yang et al.,* 2011; *Cai et al.,* 2014; *Chen et al.,* 2014] and compared to the legacy Noah LSM [*Chen et al.,* 1996; *Chen and Dudhia,* 2001; *Ek et al.,* 2003]; significant improvements in the modeling of runoff, snow, surface heat fluxes, soil moisture, and land skin temperature were noted. Although the WRF/Noah-MP modeling system includes a Ball-Berry stomatal resistance-based [*Ball et al.,* 1987] photosynthesis scheme with a dynamic vegetation model [*Dickinson et al.,* 1998], it only represents a generic type of crop. However, such a generic type of crop growth does not discern growth characteristics (planting dates, growing season, partition of dry matters, etc.) among difference crop species such as winter wheat (*Triticum aestivum)*, corn (*Zea mays*), and soybean (*Glycine max*) and therefore produces large errors in seasonal evolution of crop phenology (i.e., leaf area index).

Previous studies [*Levis et al.,* 2012; *Lu et al.,* 2015; *Harding et al.,* 2015] have explored the impact of modeling crop growth in CLM on GCM and WRF simulations. However, Noah and Noah-MP are two of the most commonly used land models in the community WRF modeling system, as well as in a suite of operational models at National Centers for Environmental Prediction (NCEP). Adding the crop growth modeling capability is critical not only for the widely used WRF/Noah-MP coupled system but also to transitioning this enhanced Noah-MP into NCEP operational models to for seasonal prediction. Moreover, Noah-MP and CLM are conceptually different land models. In CLM, each subprocess is treated in a deterministic way, while Noah-MP has multiple options (i.e., parameterization schemes) for key physical processes such as hydrology, snow, and vegetation-related processes. Even though the development of Noah-MP-corn and Noah-MP-soybean described in this study is largely similar to those done within CLM or such global community models, we consider this effort in as a first step to build a crop-ensemble modeling framework for mesoscale weather and regional hydroclimate perspective. Modeling crop growth is a complex task, because it depends on crop genotypes and regions of planting. We anticipate using this framework to accommodate, for instance, other corn species such as Chinese spring corn, Indian, and European maize, which would not be possible without the multiparameterization framework such as in Noah-MP.

In addition, agriculture is highly influenced by weather and climate. Studies of food security under a changing climate highlight an increasing demand for large-scale crop growth simulations [*Hansen and Jones*, 2000; *Niyogi and Andresen*, 2011; *Rosenzweig et al.,* 2013; *Takle et al.,* 2014; *McDermid et al.,* 2015; *Deryng et al.,* 2016]. Several studies have been conducted on large-scale crop simulations using traditional crop models [e.g., *Rosenzweig et al.,* 2014; *Elliott et al.,* 2015; *Liu et al.,* 2015]. However, traditional crop models are not able to fill the increasing demand for high spatiotemporal resolution regional agroclimatic related products. This is because (i) traditional crop models (e.g., DSSAT (Decision Support System for Agrotechnology Transfer) [*Jones et al.,* 2003] and Hybrid-Maize [*Yang et al.,* 2004]) were developed to simulate crop growth at the field scale, and limitations exist in conducting simulations at regional scales; (ii) lack of information on whether these models can represent the impact of spatial heterogeneity of climate variability on yield [*Doering et al.,* 2002; *Niyogi et al.,* 2015]; and (iii) while conducting simulations at a larger spatial scale, there are significant computational challenges, which are usually time consuming and need third-party software to drive the crop models in a coupled automated format.

More importantly, previous large-scale crop yield simulations using traditional crop models only reflected impacts of climate on yield, and neglected effects of crops on land-atmospheric interactions, which in turn, can potentially impact crop growth development [*Ramankutty et al.,* 2006; *Pielke et al.,* 2007]. Therefore, developing a computationally efficient and flexible spatiotemporal resolution regional crop growth modeling capability in WRF is necessary. Enhanced regional simulations of crop-atmospheric interactions are not only crucial to improving WRF model performance and the assessment of weather and climatic variability impacts on crop yields but can also help explain the two-way interactions between weather and crops.

The first critical step in the development of a coupled WRF-Crop modeling system is to build the Noah-MP-Crop model, based on the framework of Noah-MP, and evaluate it with field data. This paper describes the development of the dynamic crop growth model in Noah-MP, discusses a new lookup table with parameters required to execute the Noah-MP-Crop model, and the evaluation of Noah-MP-Crop against long-term field data sets, including leaf area index (LAI), surface fluxes, and biomass. Results summarized in this paper focus on the development of corn and soybean (two major crop types in the U.S. Midwest) crop models as the first

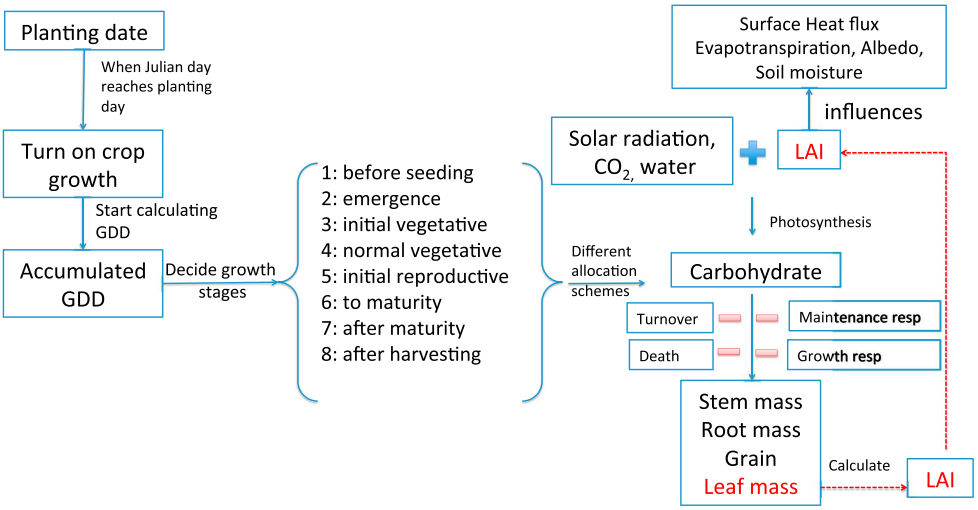

Figure 1. Flowchart of the Noah-MP-Crop model. ("LAI" and "leaf mass" marked as red color for emphasizing the calculation process and the role of LAI in the model simulations).

step in establishing a general crop-modeling framework in WRF/Noah-MP-Crop. This study is necessary for future modeling studies with WRF to assess how croplands influence the atmosphere, to explore the possibilities of improving weather forecasting via enhanced cropland representation, and to provide in-season regional crop yield simulation products.

2. Description of the Noah-MP-Crop Model

The new Noah-MP-Crop model is based on the Noah-MP model by including dynamic crop-specific growth processes to allocate the carbohydrate product from photosynthesis into different parts of a crop during the growing season. The dynamic crop growth model also calculates time-varying leaf area index (LAI), which in turn directly impacts the surface radiation, photosynthesis process, soil moisture, and surface energy fluxes. The changes in the partition of sensible heat flux and latent heat flux will affect weather/climate predictability when coupled with atmospheric models [*Jiang et al.,* 2009; *MacKellar et al.,* 2009]. Figure 1 shows the flowchart of model building blocks, while the major equations appear in Appendix A.

Noah-MP contains a separate vegetation canopy defined by a canopy top and bottom, crown radius, and leaves with prescribed dimensions, orientation, density, and radiometric properties. The canopy employs a two-stream radiation transfer approach along with shading effects necessary to achieve proper surface energy and water transfer processes including undercanopy snow processes [*Dickinson*, 1983; *Niu and Yang*, 2004]. Noah-MP contains a multilayer snowpack with liquid water storage and melt/refreeze capability and a snow-interception model describing loading/unloading, melt/refreeze capability, and sublimation of canopy-intercepted snow [*Yang and Niu*, 2003; *Niu and Yang*, 2004]. Multiple options are available for surface water infiltration and runoff and groundwater transfer and storage including water table depth to an unconfined aquifer [*Niu et al.,* 2007; *Barlage et al.,* 2015].

Noah-MP is able to predict vegetation growth by combining a Ball-Berry stomatal resistance [*Ball et al.,* 1987; *Niyogi et al.,* 2009], a photosynthesis scheme [*Collatz et al.,* 1991; *Bonan*, 1996], and a dynamic vegetation model [*Dickinson et al.,* 1998] that allocates carbon to various parts of vegetation (leaf, stem, wood, and root) and soil carbon pools (fast and slow). Photosynthesis is calculated separately for sunlit and shaded leaves and controlled by three rate-limited processes: light-limited, carboxylase-limited (Rubisco-limited), and export limited (for C3 plants). The model is capable of distinguishing between C3 and C4 photosynthesis pathways and defines vegetation-specific parameters for plant photosynthesis and respiration [*Collatz et al.,* 1991; *Oleson et al.,* 2008; *Niu et al.,* 2011]. Within Noah-MP, these processes are controlled by vegetation-type specific parameters that are read into the model through a lookup parameters table. To represent seasonal vegetation evolution, the current Noah-MP users can either use the prescribed LAI or rely on the generic dynamic

Table 1. The Growth Stages of Corn and Soybean in the Noah-MP-Crop Model[a]

Agronomic Stages of Corn (Soybean)	MP-Crop Stages	GDD Used in This Study
~VE (VE)	From planting to emergence	50 (60)
~V15 (V12)	Initial vegetative	625 (675)
~VT (R1)	Normal vegetative	933 (1183)
~R2 (R3)	Initial reproductive	1103 (1253)
~R6 (R8)	Physiological maturity	1555 (1605)

[a]GDD is 10C based. Iowa State University methods were used as references for corn and soybean agronomic growth stages [*Ritchie et al.,* 1997; *Pedersen*, 2004].

vegetation module, which does not differentiate the phenology of specific crop growth such as corn and soybean.

The Noah-MP-Crop model uses the Noah-MP photosynthesis model. To simulate the biomass of grain/yield (an important variable for the agricultural community) and be consistent with empirical crop models (e.g., Hybrid-Maize model) [*Yang et al.,* 2004], Noah-MP-Crop uses carbohydrate flux instead of carbon flux in Noah-MP. Crop-growth models are implemented in Noah-MP-Crop to simulate the seasonal evolution of various biomasses (e.g., root mass, leaf mass, and grain mass) of different crop types. In this paper, a generic framework was developed and tested with a focus on the simulation of two major crop types in the U.S.: corn and soybean. This choice is motivated by the preponderance of the two crops over the central U.S. and because of the availability of observed data for model development and validations.

Agronomically, corn and soybean are usually characterized with two major development stages: vegetative (V) stages and reproductive (R) stages. For example, during corn vegetative stages, the crop focuses on the growth of leaf and stalk, and during reproductive stages, the crop focuses on the development of tassel and ears [*Abendroth et al.,* 2011]. The key growth stages of corn include Emergence (VE), 6 collars (V6), 15 collars (V15), tassel (VT), silking (R1), blister (R2), and physiological maturity (R6) [*Ritchie et al.,* 1997]. The key growth stages of soybean are as follows: emergence (VE), cotyledon (VC), first trifoliate (V1), *n*th trifoliate (Vn), beginning bloom (R1), full pod (R4), full seed (R6), and full maturity (R8) [*Pedersen*, 2004]. In Noah-MP-Crop these agronomic crop growth stages were represented by five plant growth stages (PGS): (1) from planting to emergence (PGS2), (2) initial vegetative (PGS3), (3) normal vegetative (PGS4), (4) initial reproductive (PGS5), and (5) to physiological maturity (PGS6). The relationship between the modeling stages and agronomical growth stages is listed in Table 1. Considering field management, there are three additional stages beyond the growing season: before planting (PGS1), from maturity to harvesting (PGS7), and after harvesting (PGS8). Management factors were incorporated into crop PGS because it is anticipated that they (e.g., harvesting) can change the ground vegetation cover. The above eight crop stages allow modeling of the entire crop growth cycle (see Figure 1).

Since the phenology development of crops depends on temperature, crop modelers normally use the accumulated growing degree days (GDD) as a heat unit to indicate crop growth stages. Following the approach used in classical crop models (DSSAT and Hybrid-Maize), accumulated GDD was also used to determine crop growth stages (equations A1, A2, A3). Different crop types and hybrid cultivars require different accumulated GDD from planting to physiological maturity [*Niyogi et al.,* 2015]. In Noah-MP-Crop, users can easily customize the accumulated GDD requirements for different growth stages in the lookup table (Table 2). Field management practices (e.g., planting and harvesting dates) are prescribed in Noah-MP-Crop lookup table (Table 2) based on site observations. It is assumed that after harvesting, there is no aboveground biomass left in the field.

Through the photosynthesis process, photosynthetically active radiation is used to convert atmospheric carbon dioxide into carbohydrate in leaves (equation (A4)). The total assimilated carbon then is allocated to different carbon pools (leaf, stem, root, grain, and soil). Maintenance respiration and growth respiration are inevitable costs of photosynthesis process [*Cowan and Givnish*, 1986], and turnover and senescence additionally cause the loss of carbohydrate in the crops. In different crop growth stages, the allocation of carbohydrate fluxes and respiration rates varies, as does the turnover and senescence rate (equations A5, A6, A7, A8). The different parametric coefficients are described in the crop-specific parameters lookup table (Table 2). During vegetative periods, the carbohydrate fluxes for corn, for example, are mainly allocated to leaf, stem, and root, and during the reproductive period, the carbohydrate fluxes are mainly allocated to grain. At the mature reproduction stage, carbohydrate fluxes are only allocated to grain and root, and leaves are continually senescent, and the carbohydrate in stems and roots will be partially translocated to grain [*Yang et al.,* 2004].

Table 2. Parameters in New User Customized Table in the Noah-MP-Crop Model[a]

Parameters	Description	Values for Corn (Soybean)	Equations
PLTDAY	Planting day (in Julian day format)	111 (131)	(A3)
HSDAY	Harvesting day (in Julian day format)	300 (280)	(A3)
GDDTBASE	Base temperature for GDD accumulation (c)	10 (10)	(A1)
GDDTCUT	Upper temperature for GDD accumulation (c)	30 (30)	(A1)
GDDS1	GDD from seeding to emergence	50 (60)	(A3)
GDDS2	GDD from seeding to initial vegetative	625 (675)	(A3)
GDDS3	GDD from seeding to normal vegetative	933 (1183)	(A3)
GDDS4	GDD from seeding to initial reproductive	1103 (1253)	(A3)
GDDS5	GDD from seeding to physical maturity	1555 (1605)	(A3)
Q10MR	Q10 for maintenance respiration	2.0 (2.0)	(A5)
FOLN_MX	Foliage nitrogen concentration (%)	1.5 (1.5)	(A5)
LEFREEZ	Characteristic T for leaf freezing (K)	268 (268)	(A7)
BIO2LAI	Leaf area per living leaf biomass (SLA)	0.015 (0.030)	(A9)
LFMR25	Leaf maintenance respiration at 25c (μmol co2/m**2/s)	1.0 (1.0)	(A5)
STMR25	Stem maintenance respiration at 25c (μmol co2/kg bio/s)	0.05 (0.05)	(A5)
RTMR25	Root maintenance respiration at 25c (μmol co2/kg bio/s)	0.05 (0.05)	(A5)
GRAINMR25	Grain maintenance respiration at 25c (μmol co2/kg bio/s)	0 (0)	(A5)
FRA_GR	Fraction of growth respiration	0.2 (0.2)	(A6)
DILE_FC(PGS)	Coefficient for leaf temperature stress death (1/s)	PGS = 5: 0.5 (0.5) PGS = 6: 0.5 (0.5)	(A7)
DILE_FW(PGS)	Coefficient for leaf water stress death (1/s)	PGS = 5: 0.2 (0.2) PGS = 6: 0.2 (0.2)	(A7)
LF_OVRC(PGS)	Leaf turnover coefficient (1/s)	PGS = 5: 0.2 (0.2) PGS = 6: 0.3 (0.3)	(A7)
ST_OVRC(PGS)	Stem turnover coefficient (1/s)	PGS = 5: 0.2 (0.12) PGS = 6: 0.3 (0.06)	(A7)
RT_OVRC(PGS)	Root turnover coefficient (1/s)	PGS = 5: 0.12 (0.12) PGS = 6: 0.06 (0.06)	(A7)
LFPT(PGS)	Fraction of carbohydrate flux to leaf	PGS = 3: 0.36 (0.4) PGS = 4: 0.1 (0.2)	(A6) and (A8)
STPT(PGS)	Fraction of carbohydrate flux to stem	PGS = 3: 0.24 (0.2) PGS = 4: 0.6 (0.5)	(A6) and (A8)
RTPT(PGS)	Fraction of carbohydrate flux to root	PGS = 3: 0.4 (0.4) PGS = 4: 0.3 (0.3) PGS = 5: 0.05 (0.05)	(A6) and (A8)
GRAINPT(PGS)	Fraction of carbohydrate flux to grain	PGS = 5: 0.95 (0.95) PGS = 6: 1 (1)	(A6) and (A8)

[a]PGS means plant growth stage; some parameters have different values for each growth stages.

Within the Noah-MP framework, leaf density is a primary link to atmosphere/cropland interactions, and an accurate estimation of LAI is critical to calculating surface latent heat fluxes through crop transpiration and hence for correctly partitioning incoming energy into surface sensible heat flux and latent heat flux. LAI influences photosynthesis, albedo, sensible heat flux, latent heat flux, net radiation soil heat flux/surface energy storage, and also the green leaf biomass in the prognostic solutions. The LAI in Noah-MP-Crop is calculated by multiplying green leaf biomass with specific leaf area (SLA, leaf area per living leaf biomass $m^2\ g^{-1}$). In reality SLA varies with crop and cultivar types (equation (A9)) and can also vary temporarily during the growing season. In Noah-MP-Crop, due to the lack of observations and simple mathematical relation, we assume the SLA to be constant throughout the growing season. This assumption is used in many modeling studies, and the value can be recalculated in the future if detailed spatiotemporal leaf mass and LAI data are available to develop a functional relation.

Compared to the original dynamic vegetation module and prescribed LAI methods in Noah-MP, one highlight of Noah-MP-Crop is the ability to simulate grain biomass, which is the "yield" of crops when they reach physiological maturity. The yield simulations can be potentially used in agroclimatic assessments as well as future yield predictions.

As will be discussed below, this initial version of Noah-MP-Crop was developed and calibrated based on observations in the U.S. Corn Belt. Model calibrations may be necessary when users apply it to different

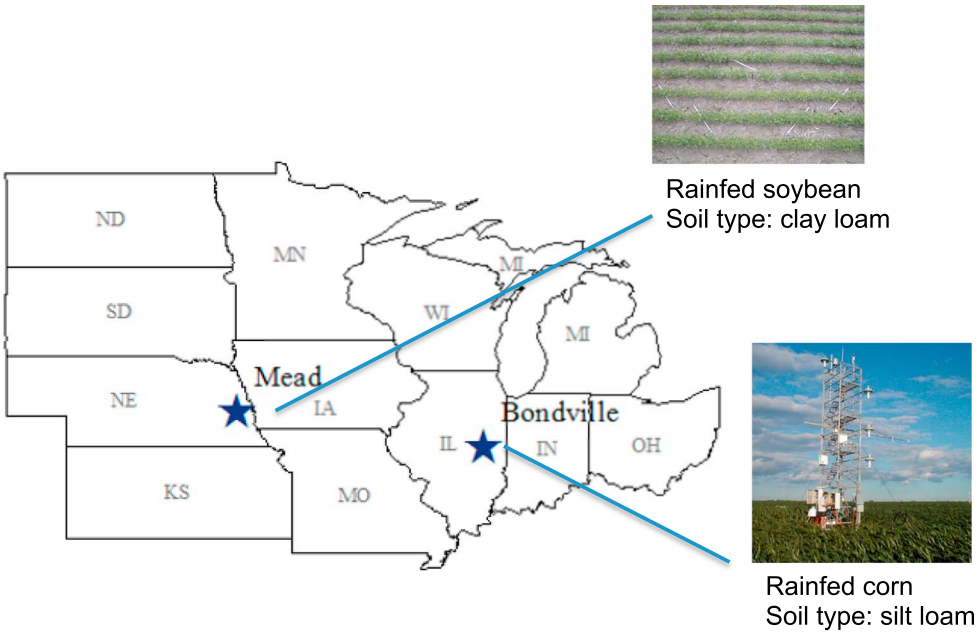

Figure 2. Experimental AmeriFlux sites. (Photo credits: AmeriFlux).

regions. Also, different regions have different management strategies (e.g., planting date and harvest date). Therefore, the new crop-specific parameters lookup table (Table 2) needs to be modified to accommodate those differences.

3. Observation Site Description and Model Experiments

The Noah-MP-Crop model for simulating corn and soybean growth was evaluated against field observations. Data were obtained from two long-term Ameriflux sites [http://ameriflux.ornl.gov/]: Bondville, IL (US-Bo1, 40.00°N, 88.29°W), and Mead, NE (US-Ne3, 41.18°N, 96.44°W). These two sites are typically used to test crop models. Data from the Bondville site were used for evaluating corn simulations, and data from the Mead site were used for evaluating soybean simulations. Half hourly and hourly in situ meteorological forcing data were used to drive the off-line Noah-MP-Crop model.

The Bondville (US-Bo1, Figure 2) and Mead sites (US-Ne3, Figure 2) are characterized by rainfed no-till management with annual rotation between corn and soybean. The fields are predominately characterized as silt loam over Bondville and clay loam over Mead. For both sites, observed hourly sensible heat flux (H), latent heat flux (LE), top layer (0.1 m), and second layer (0.1–0.4 m) soil moisture were used to evaluate the model. Moreover, observed biomass data at the Bondville site (e.g., LAI, green leaf mass, stem mass, and grain mass) were used to assess simulated crop growth characteristics of Noah-MP-Crop simulations for 2001, 2003, and 2005 when corn was planted. Similarly, available biomass observations at the Mead site (e.g., LAI and total aboveground biomass) were used to compare against Noah-MP-Crop simulations for 2002, 2004, and 2006 when the field grew soybeans. Planting and harvest dates at these two sites varied in different years based on the observations listed in Table 3, and the users will need to modify them for different regions.

Noah-MP-Crop-based corn simulations were conducted for the Bondville site for 2001 to calibrate crop growth model parameters. Using these 2001 default values, simulations were then performed for 2003 and 2005 by only changing the planting dates and SLA calculated from the observed data. Simulations conducted with the Noah-MP-Crop model were named "MP-CROP." For comparison, Noah-MP default simulations were also conducted for the same periods using monthly prescribed LAI (referred to as MP-TBLAI) and using the current Noah-MP dynamic vegetation option (referred to as MP-DVEG). There are a total of nine numerical experiments each for corn and soybean, respectively. To quantify differences in results from those experiments, mean absolute error (MAE) was used.

Table 3. Data From Ameriflux Sites

Sites	Category	Parameters	Period
Bondville, IL	Inputs	Meteorological forcing (half hourly)	2001–2006
		Planting dates of corn	2001, 2003, and 2005
		Leaf area per living leaf biomass (SLA)	2001, 2003, and 2005
	Validations	Surface heat fluxes (half hourly)	2001, 2003, and 2005
		0–10 cm soil moisture (half hourly)	
		10–40 cm Soil moisture (half hourly)	
		Leaf area index (LAI)	
		Biomass of leaf, stem, and grain	
Mead, NE	Inputs	Meteorological forcing (hourly)	2001–2006
		Planting dates of soybean	2002, 2004, and 2006
		Leaf area per living leaf biomass (SLA)	2002, 2004, and 2006
	Validations	Surface heat fluxes (hourly)	2002, 2004, and 2006
		0–10 cm Soil moisture (hourly)	
		10–40 cm Soil moisture (hourly)	
		Leaf area index (LAI)	
		Total above ground biomass	

4. Results and Discussion

4.1. Simulated Seasonality of Crop Growth Characteristics

Correctly simulating GDD is important in determining not only for different Noah-MP PGS but also for a broad range of users, especially agronomists, to estimate crop growth stages. As shown in Figure 3, there is notable year-to-year variability in GDD during the growing conditions (from planting to maturity). At the corn site in Bondville (Figure 3a), starting from June, GDD increases in 2005 faster than in 2001 and 2003. At the soybean site in Mead (Figure 3b), starting from late June, GDD increases slower in 2004 than in 2002 and 2006. Because GDD is a function of air temperature, higher average temperature leads to higher GDD. Given the same genetic parameters of crops, higher GDD in 2005 at the Bondville site means that corn reaches successive growth stages at a faster pace than in the other 2 years. Similarly, the lower GDD in 2004 at the Mead site indicates that in 2004, soybeans have a slower developing growth than in the other 2 years. For example, in this study, GDD for corn maturity is set to 1555 based on *Neild and Newman* [1987]. With this criterion, corn reaches the maturity stage on day of year (DOY) 264 in 2001, DOY 267 in 2003, and DOY 247 in 2005 (Figure 3a). Therefore, higher GDD in the 2005 growing season leads to a maturity stage 20 days earlier than the other years.

The GDD of soybean to finish vegetative development is set to 1183 based on *Kumar et al.* [2008], and the vegetative development was completed on DOY 222 in 2002, DOY 221 in 2006, and DOY 242 in 2004 (Figure 3b). In 2004, soybean needed 20 more days for vegetative development compared to 2002 due to the slower accumulation of GDD. As discussed below, the effects of a longer vegetative period are reflected in higher LAI (Figure 4b). These results highlight the decisive role of temperature and the use of GDD in

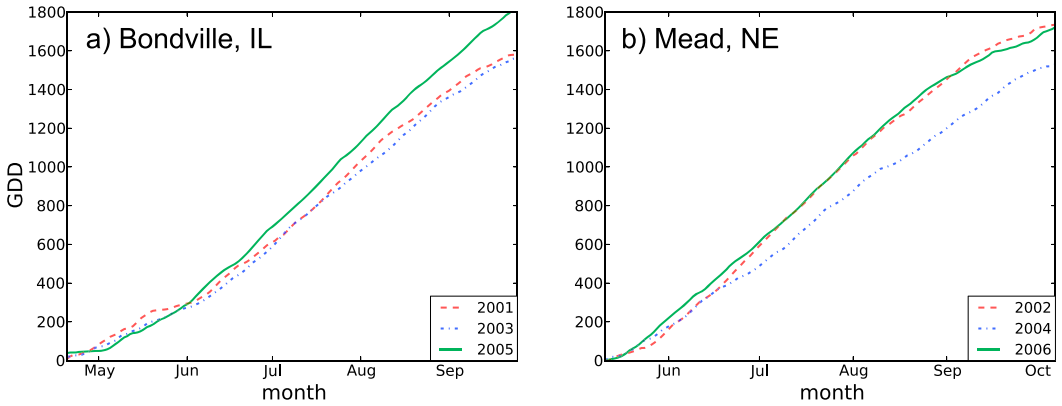

Figure 3. Growing degree days (GDD) of growing season for the (a) Bondville site and the (b) Mead site.

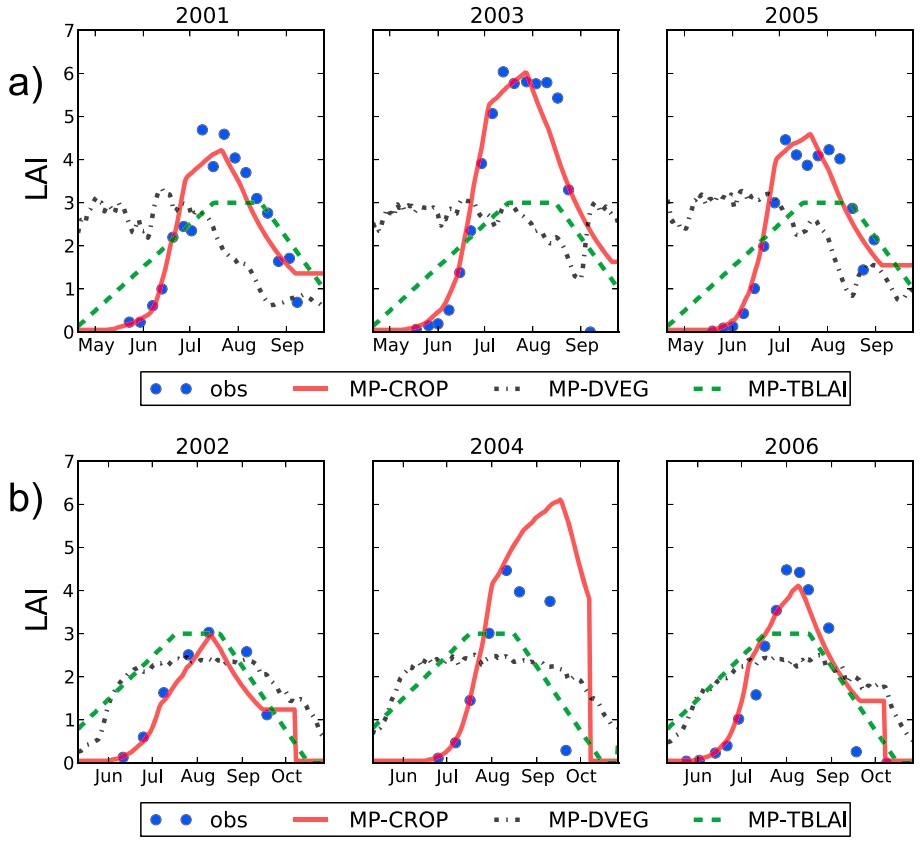

Figure 4. (a) Comparisons of simulated LAI for corn at the Bondville site. (b) Comparisons of simulated LAI for soybean at the Mead site. (obs: observations, collected form Ameriflux site).

determining crop growth characteristics. Therefore, the ability to capture the annual variability of GDD and its association with crop growing stages is critical to Noah-MP long-term (such as multiyear time scale) simulations.

The amount of crop leaves also modulates canopy radiation, turbulence transfer, and plant transpiration. As shown in Figure 4a, using the default table-based green LAI approach (MP-TBLAI) captures the general trend but overestimates spring LAI and underestimate summer LAI for corn. Meanwhile, MP-DVEG cannot capture the general corn growing seasonality and resulted in a premature reproductive stage (starting in June compared to July in field observations) resulting in rapid reduction of LAI in July. Compared to these two existing Noah-MP capabilities, the new Noah-MP-Crop has superior performance in reproducing observed seasonal variations and LAI amounts for corn fields. The 3 year averaged LAI MAE of MP-CROP (corn) is 0.4, much lower than that simulated by MP-DVEG (1.98) and MP-TBLLAI (1.19) (Table 4).

For soybean simulation (Figure 4b), the vegetative growing seasons in both MP-TBLAI and MP-DVEG 3 year simulations start about 1 month too early, and the reproductive stage lasts too long. As with the corn simulations, MP-CROP is much better at capturing the start and end of the vegetative growing and reproductive growing seasons and produces better agreement with LAI observations. As aforementioned, the slower increase of GDD in 2004 resulted in overestimated LAI and prolonged the length of the vegetative and reproductive stages. The 3 year averaged LAI MAE of MP-CROP (soybean) is 0.63 and is lower than that produced by MP-DVEG (1.26) and MP-TBLAI (1.14) (Table 4).

These results show the limitations of using GDD alone to predict crop growth stages since the accumulated GDD criteria used in this study and other studies [e.g., *Levis et al.,* 2012] are the mean value of long-term GDD climatic data. Under "normal" climatic conditions, the model performs well using the mean GDD. However, the long-term mean GDD requirements may not reflect the impacts of climate variability and results in reduced accuracy of predicting crop growth stages under abnormal climatic conditions. For example, in

Table 4. MAE of LAI Simulations (Unit: $m^2\ m^{-2}$)

Sites	Crop	Year	MP-CROP	MP-DVEG	MP-TBLAI
Bondville,IL	Corn	2001	0.43	1.60	0.77
		2003	0.38	2.50	1.83
		2005	0.38	1.83	0.96
		Average	0.40	1.98	1.19
Mead,NE	Soybean	2002	0.25	0.84	0.82
		2004	1.26	1.59	1.44
		2006	0.38	1.33	1.18
		Average	0.63	1.26	1.14

the presence of drought, the GDD criterion for each PGS tends to be lower than normal conditions, while under anomalous wetting, the GDD requirements will be higher [*Miller et al.,* 2001]. *Yang et al.* [2004] pointed out that for corn under optimal water conditions, the actual GDD values to reach the silking stage tend to be lower than its climatic mean value. In the current version of Noah-MP-crop, GDD has not yet been combined with water availability or other variables needed to predict crop growth stages due to the lack of information required to quantify the impacts of climate variability on GDD requirements. The rapid drop of LAI in late October in the MP-CROP simulations is due to harvesting.

Figure 4 shows the differences in growing stages as well as in the peak values of LAI between corn and soybean. In our study sites, the plantings dates of corn (soybean) start in early May (June). LAI of corn (soybean) peaks in July (August), and the maximum LAI of corn is higher than that of soybean for those specific years. By using distinctive planting function for corn and soybean, Noah-MP-Crop is able to capture these differences in LAI during various crop growth stages, which is critical for land-atmospheric interactions.

As demonstrated, so far, the Noah-MP-Crop model is able to capture the seasonal and annual variability of LAI by incorporating planting, harvesting, and crop growth functions of corn and soybean. Also noted is the ability of the model to differentiate LAI characteristics between C3 (soybean) and C4 (corn) crops, while the MP-TBLAI and MP-DVEG approach shows similar LAI maximum values for both sites. The corn LAI simulations at the Mead site and the soybean simulations at the Bondville site were validated using the Noah-MP-Crop default crop genetic parameters. The results (Figure S1 in the supporting information) indicate that the model is able to conduct studies at different locations with minimum calibration.

4.2. Impacts of LAI on Surface Heat Fluxes During the Growing Season

With the enhanced simulations of LAI, cascading impacts on the exchange of energy and water between the cropland surface and the atmosphere during the crop growing season were expected. For corn simulations at the Bondville site, the monthly diurnal pattern of site-observed sensible heat flux (H) is generally well captured by each of the three model options (Figure 5a). MP-CROP shows improved performance in simulating H, especially for May–August. For instance, both the observations and MP-CROP simulations show low values of LAI in May. Compared to the MP-DVEG and MP-TBLAI simulations, lower LAI in observations and MP-CROP simulations during the early corn growing stage allows more solar energy to reach the ground surface resulting in higher sensible heat flux [*Hardwick et al.,* 2015]. In July and August, high values of LAI can be seen in the observations and MP-CROP simulations. Higher LAI reduces H in the summer, causing the "cooling effect" of croplands [*Bonan*, 2001; *Lobell et al.,* 2006], and this cooling effect is well captured by MP-CROP. The MAE of daytime sensible heat flux in MP-CROP at the Bondville corn site is 36.1 $W\ m^{-2}$ (Table 5), which is significantly lower than that of MP-DVEG (63.8 $W\ m^{-2}$) and MP-TBLAI (50.2 $W\ m^{-2}$). The focus was on daytime MAE instead of daily averaged MAE, because the period of interest is when crop transpiration is active and surface heat flux values are high. For latent heat flux (LE) simulations (Figure 5b), three model options also captured the seasonal trend of the diurnal cycle of LE: high in peak growing seasons (June–August) and low in the early growth and harvesting stages. MP-CROP shows improvement in simulating the LE in early growing season: May and June. For example, the MAE in MP-CROP for May in simulating LE is 51.1 $W\ m^{-2}$, which is 47% lower than MP-DVEG and 25% lower than MP-TBLAI (Table 5). Nevertheless, the improvement in simulating LE in MP-CROP is not as notable as improving H, and one possible reason is that the dynamic root depth and density were not parameterized in the Noah-MP-Crop model, which suggests estimation of the seasonal access to soil water could have deficiencies. In the model, crop rooting depth is set as 1 m through the whole growing season, which limits the interaction between root and soil moisture as indicated in other studies [*Gayler et al.,* 2014]. In general, the LE simulation at the beginning of the season is reasonable so we that think the eventual inclusion of the root-water dynamics will improve the middle to late season partitioning between H, LE, and G.

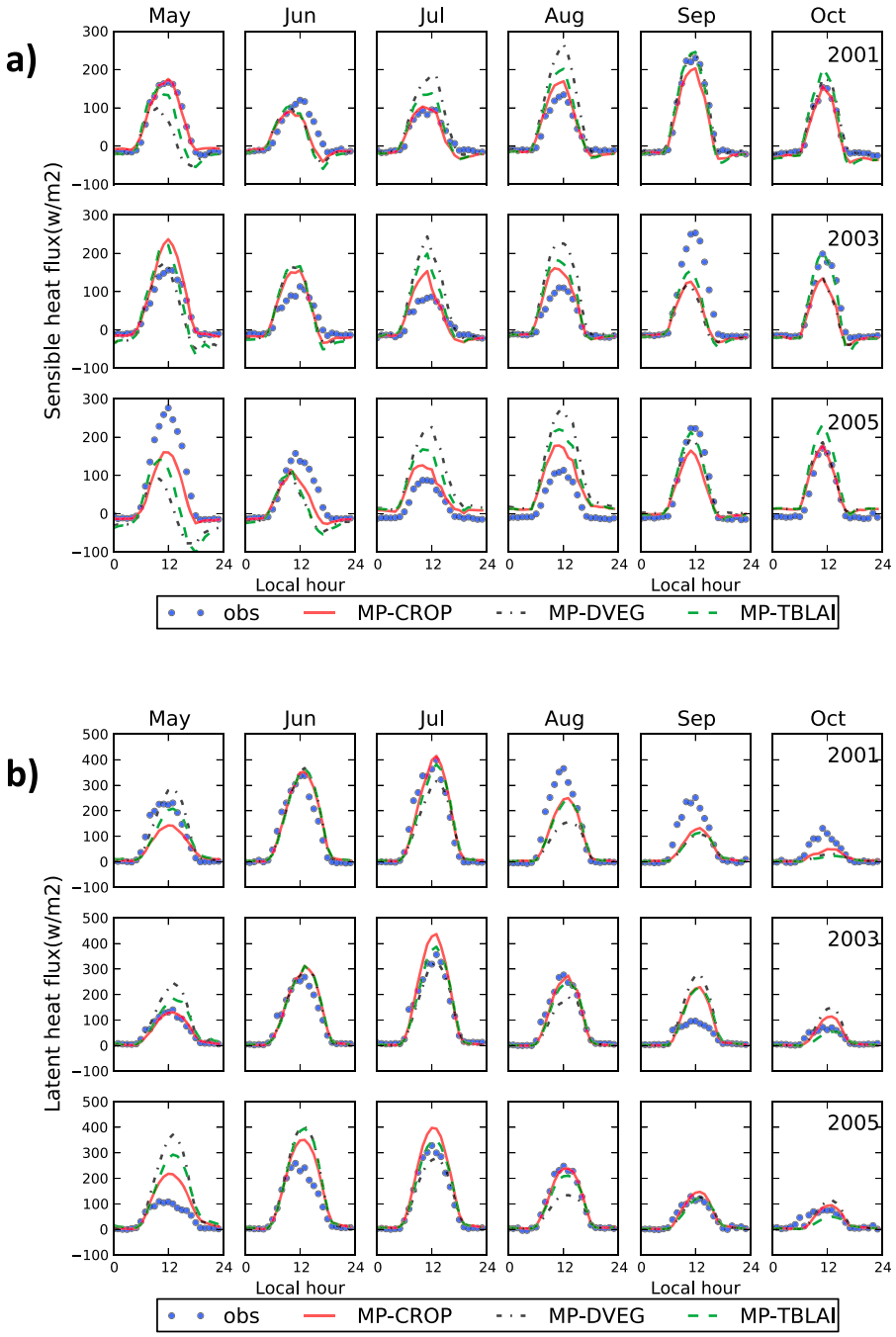

Figure 5. (a) Comparison of simulated sensible heat flux (H) for corn at the Bondville site. (obs: observations, collected form Ameriflux site). (b) Comparison of simulated latent heat flux (LE) for corn at the Bondville site. (obs: observations, collected form Ameriflux site).

For soybean simulations at the Mead site, three model options captured the general seasonal variations in H, and MP-CROP shows enhanced performance in May and June (Figure 6a and Table 5). For example, in June, the MAE of MP-CROP is 33.3 W m^{-2}, which is 57% lower than the MAE of MP-DVEG and 58% lower than the MAE of MP-TBLAI. This improvement in MP-CROP is mainly due to the fact that a dynamic crop growth model is able to simulate the low LAI (Figure 4b) during the early soybean growing season where current Noah-MP modeling methods failed. From July to October, the three model options show similar performance and good agreement with observations (Table 5). The average growing season daytime MAE

Table 5. MAE of Sensible Heat Flux and Latent Heat Simulations During the Daytime (8 A.M. to 6 P.M., 3 Year Average, Unit: W m^{-2})

Sites	Crop	Month	MP-CROP	MP-DVEG	MP-TBLAI
Bondville, IL	Corn	May	42.2	94.2	74.5
Sensible heat flux		June	39.6	51.1	53.4
		July	24.5	77.9	48.2
		August	36.9	94.4	56.2
		September	50.7	40.8	38.4
		October	22.9	24.7	30.7
		Average	36.1	63.8	50.2
Mead,NE	Soybean	May	55.6	70.7	82.1
Sensible heat flux		June	33.3	76.8	79.2
		July	17.8	20.1	18.3
		August	30.4	35.0	32.1
		September	52.0	48.8	47.7
		October	48.4	46.5	49.1
		Average	39.6	49.6	51.4
Bondville, IL	Corn	May	51.1	95.7	68.1
Latent heat flux		June	48.7	59.1	60.1
		July	49.9	40.4	36.5
		August	32.2	79.8	39.8
		September	53.7	66.6	57.9
		October	25.7	37.2	31.4
		Average	43.5	63.1	49.0
Mead,NE	Soybean	May	97.9	116.1	120.1
Latent heat flux		June	83.0	135.3	130.6
		July	48.8	50.9	47.7
		August	23.1	32.0	27.8
		September	61.9	70.1	63.0
		October	61.1	58.0	60.0
		Average	62.6	77.1	74.2

for the H simulations was as follows: 39.6 W m^{-2} (MP-CROP), 49.6 W m^{-2} (MP-DVEG), and 51.4 W m^{-2} (MP-TBLAI). Similar to the H simulations, the LE MP-CROP simulations (Figure 6b) show better performance in May and June than MP-DVEG and MP-TBLAI. The LE MAE MP-CROP in June is 83 W m^{-2}, which is 39% lower than MP-DVEG and 36% lower than MP-TBLAI. From July to August, the three model options show very similar and good performance in simulating LE. In September and October, the three model options overestimate LE. The average growing season daytime MAE of the LE simulations was as follows: 62.6 W m^{-2} (MP-CROP), 77.1 W m^{-2} (MP-DVEG), and 74.2 W m^{-2} (MP-TBLAI).

In summary, for the corn site (Bondville) and the soybean site (Mead), MP-CROP significantly improved the simulation of surface heat fluxes, especially surface sensible heat fluxes in the first half of the crop growing season (May–July) due to its ability to capture the observed evolution of LAI.

4.3. Soil Moisture and Soil Temperature

A comparison of soil moisture simulations by the three Noah-MP model options with observations for the Bondville site is shown in Figure 7a. MP-DVEG, MP-TBLAI, and MP-CROP produce similar seasonal trends with observations responding to precipitation and evapotranspiration. Daily fluctuations in layer 1 are more frequent than layer 2, as expected. The similarity in simulated soil moisture can perhaps be attributed to the fact that all three model options use the same prescribed rooting depth, and the model lacks a dynamic root development scheme, which is a priority for future Noah-MP-Crop model development. The results indicate that at these two sites, the Noah-MP model can capture weekly and seasonal variability but still underestimates soil moisture. The underestimations may be caused by uncertainties in the observations, use of a single soil type for all soil layers in the model, the limitations in simulating soil moisture dynamics/soil physics, and the poor representation of roots. For example, the soil type of Bondville is silt loam, but in the model default setting, the maximum soil moisture of silt loam is 0.476 (m^3 m^{-3}). However, in 2003, some observations of the first layer exceeded 0.476.

Since there is a gap between modeled soil moisture and observations (Figure 7a), probability density functions (pdfs) of normalized soil moisture (Figure 7b) were compared. The equation used for normalization is as follows:

$$\Theta = \frac{\theta - \theta_{\min}}{\theta_{\max} - \theta_{\min}}$$

where Θ is normalized soil moisture, θ is the soil moisture, and $\theta_{\max}$ and $\theta_{\min}$ are the maximum and minimum soil moisture in modeled results and observations, separately. As shown in Figure 7b, the pdfs of observations have large year-to-year variability for both layer 1 and layer 2. In 2005, the pdfs of observations for low normalized soil moisture (<0.2) dominate the whole distribution of both layers. In 2001, the pdfs of observations

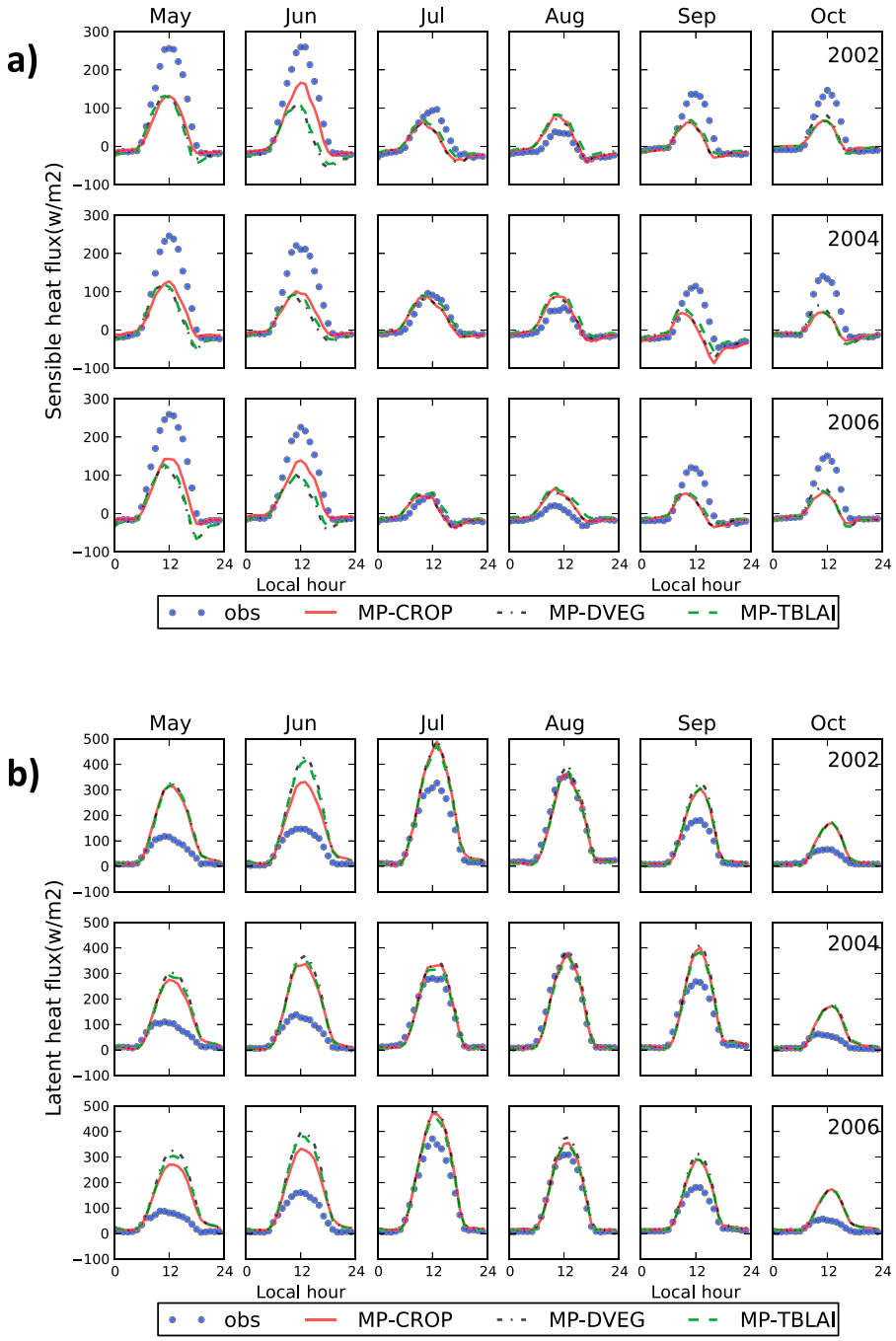

Figure 6. (a) Comparison of simulated sensible heat flux at the soybean site in Mead, NE. (obs: observations, collected form Ameriflux site). (b) Comparison of simulated latent heat flux at the soybean site in Mead, NE. (obs: observations, collected form Ameriflux site).

for high normalized soil moisture (>0.8) dominate layer two. In 2003, the pdfs tend to be normal. The three model options show similar performance in the pdfs. They are able to capture the density distribution range when the observations are normal (e.g., 2003) but fail to simulate "extreme" situations. For instance, the model cannot capture the large density of low soil moisture in 2005 or the small density of high soil moisture of layer two in 2001. The results also show the difficulties in soil moisture simulations and in comparing modeled soil moisture with observations, which is a common problem in land surface modeling [*Koster and Milly*, 1997; *Chen and Mitchell*, 1999; *Cosgrove et al.,* 2003; *Chen et al.,* 2007], because modeled soil moisture heavily

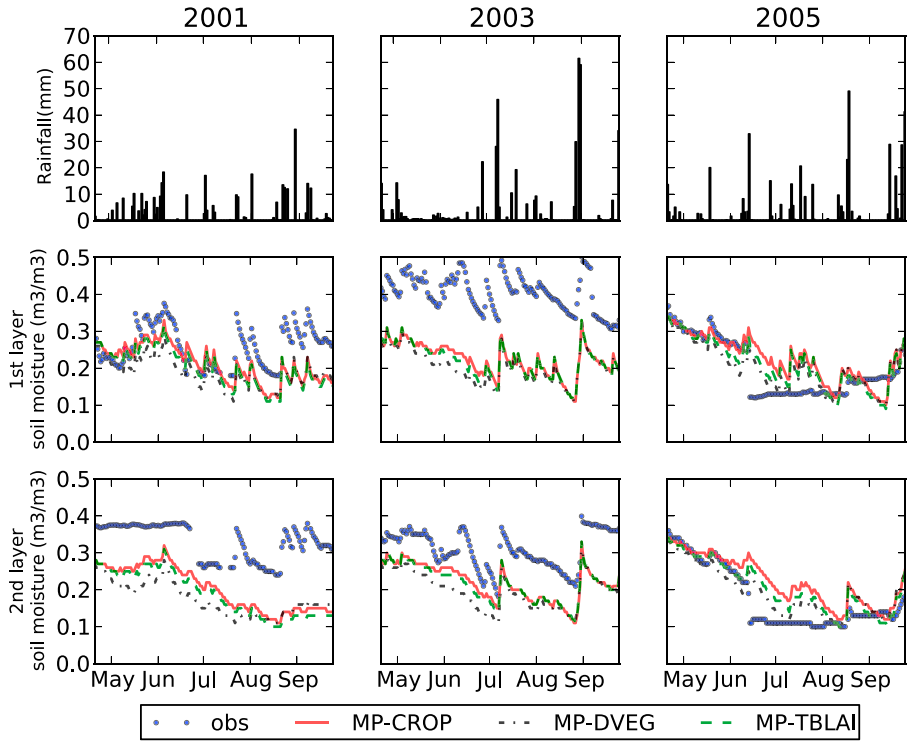

Figure 7. (a) Daily precipitation (mm, upper panel) and comparisons of simulated first soil layer (5 cm, middle panel), and second soil layer (30 cm, lower panel) soil moisture for the Bondville site. (obs: observations, collected form Ameriflux site). (b) Probability density distribution of normalized soil moisture. (obs: observations, collected form Ameriflux site). (c) Surface soil temperature (K, daily average). (d) Probability density distribution of surface soil temperature. (obs: observations, collected form Ameriflux site).

depends on how models treat evaporation-runoff processes and may have their own soil moisture dynamic ranges that are different from observations.

Despite the lack of dynamic root parameterization in Noah-MP, including crop models indeed produces discernable differences in simulated soil moisture during the growing season in the top two soil layers. Hence, to effectively assimilate soil moisture products, such as those obtained from the Soil Moisture Active Passive sensor, in agricultural regions, crop growth effects on the seasonal evolution of soil moisture may need to be taken into account.

For soil temperature, the three model options are able to replicate seasonal trends (Figure 7c). There are no obvious differences between MP-CROP, MP-DEVG, and MP-TBLAI in the early stages of the growing season (e.g., May and June). During July–September, the models tend to overestimate the surface temperature, but MP-CROP shows a smaller bias than the other two model options. Similar results can be seen in the probability density distributions (Figure 7d).

4.4. Evaluation of Noah-MP-Crop Estimated Crop Biomass and Yield

In addition to enhancing the representation of cropland-atmosphere interactions, one expected benefit of the community Noah-MP-Crop model is its ability to provide crop yield information useful for agriculture studies and management applications at regional scales in the context of computationally efficient High-Resolution Land Data Assimilation System [*Chen et al.,* 2007]. Various biomass simulated by Noah-MP-Crop at the Bondville site are shown in Figure 8a. The simulated results are remarkably close to observations, successfully capturing the rapid leaf growth in June, rapid stem growth in July, decline in leaf and stem mass at the end of July when corn starts the reproduction growth stage, and the rapid grain growth in August. The MAE of the simulated biomass is low ($<$12%, Table 6). For 2005, Noah-MP underestimated stem mass but overestimated grain mass in August. The redistribution functions between stem and grain seem to be the main factor contributing to this problem.

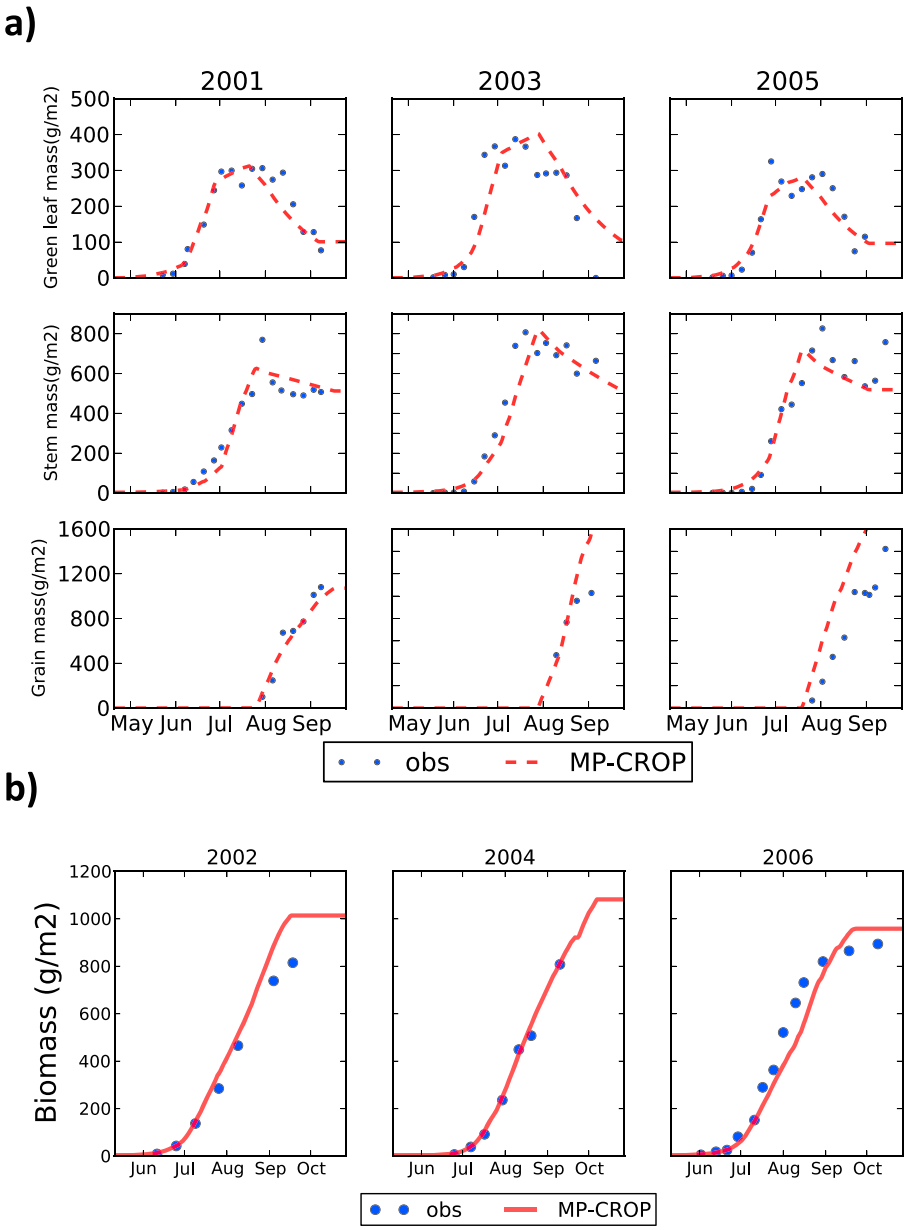

Figure 8. (a) Simulated leaf, stem, and grain biomass of corn at the Bondville site. (obs: observations, collected form Ameriflux site) (b) Simulated aboveground soybean biomass at the Mead site. (obs: observations, collected form Ameriflux site).

Since the Mead site observations only reported the total aboveground soybean biomass, the simulated leaf, stem, and grain mass were summed up to compare with observations (Figure 8b). Again, the Noah-MP-Crop model-simulated results closely followed the observed trend but tended to slightly overestimate soybean yield. Especially in 2004, the model simulates higher biomass than 2002 and 2006; we believe that this relates to the overestimation of LAI in 2004.

Table 6. MAE of Biomass Simulations (Unit: g m^{-2})

Sites	Crop	Parts	2001	2003	2005	Average
Bondville,IL	Corn	Leaf	26	50	33	36
		Stem	49	75	67	64
		Grain	75	207	427	236
			2002	2004	2006	Average
Mead, NE	Soybean	Aboveground	47	15	65	42

Note that the overarching goal for the Noah-MP-Crop model is to provide an attainable yield rather than an actual yield. Although the

impacts of water stress on yield were considered in the model, the yield loss caused by insects and weeds was not. And the model assumes that there is optimal nutrient availability. It is worth noting that the Noah-MP-Crop model shows good performance in capturing seasonal and annual biomass variability in corn during those 3 years.

Compared to traditional crop models (e.g., DSSAT and Hybrid-Maize), the Noah-MP-Crop model can be executed with fewer crop-specific input parameters and with a more flexible time step, while the traditional models only can simulate at a daily time step, which is critical for coupling it with climate and weather models. Additionally, Noah-MP-Crop includes more realistic and detailed biophysical processes than traditional crop models.

5. Conclusions and Future Work

This paper describes the development and evaluation of the Noah-MP-Crop model, as the first step toward enhancing the representation of two-way crop-atmospheric interactions in WRF. Corn and soybean growth models were incorporated into Noah-MP along with a customizable lookup table for specific crop biophysical and management parameters. Evaluated with long-term field observations, the Noah-MP-Crop model is able to capture seasonal and annual variations in corn and soybean phenology and biomass. Furthermore, it produces better agreement with observations compared to current available methods in Noah-MP. In particular, improved simulations of LAI in Noah-MP-Crop lead to improved surface heat fluxes, especially in the early period of the growing season where current Noah-MP significantly overestimated LAI. These results highlight the importance of correctly simulating the seasonal evolution of crops and its implications in affecting land-atmospheric interactions through the exchange of heat and water vapor over agricultural regions. This study also indicates the necessity of incorporating field management in Noah-MP-Crop. The addition of crop yields and GDD as model outputs expands the application of Noah-MP-Crop to regional agriculture studies. Noah-MP-Crop can be used in (1) assessment of impacts of crop growth on weather when couple with WRF and (2) regional agroclimatic analysis on the impacts of climate change/climate variability on crop yield (e.g., under Agricultural Model Intercomparison and Improvement Project's gridded modeling assessment framework) [*Elliott et al.,* 2015].

Results reveals that the relationship between GDD and crop growing stages significantly affects the simulation of crop and phenology and hence surface heat fluxes and crop biomass. However, there are limitations in the use of climatology and temperature-based GDD alone in predicting growth stages, which will restrict the model in capturing the impacts of climate variability. It is necessary to develop a new method that combines GDD with other environmental factors (e.g., water availability), to more accurately define crop growth stages. To accomplish this goal, collaboration with the agricultural community continues to be evolving. The improvement of simulated LE and soil moisture in Noah-MP-Crop is not as notable as improving surface sensible heat fluxes. We speculate that including dynamic root depth and density parameterization would enhance these aspects. To sum up, for the future improvements of Noah-MP-Crop, we will focus on the following: (1) improve the simulation of dynamic root-soil moisture interaction, (2) add irrigation function that will interact with water table and water network, and (3) continue to enhance the role of management information (planting dates and cultivar selections) in the model.

Appendix A: Major Equations in the Noah-MP-Crop Model

This appendix includes the major equations that are used in the Noah-MP-Crop model.

GDD calculation:

Basic equation:

$$\mathrm{GDD} = \frac{T_{\max} - T_{\min}}{2} - T_{\mathrm{base}}$$

GDD growing degree days;
$T_{\max}$ maximum daily temperature (C);
$T_{\min}$ minimum daily temperature (C);
T_{base} base temperature for organism (C).
Implemented equations in Noah-MP-Crop:

$$\mathrm{GDD}_i \sum_i (T_i - \mathrm{GDDTBASE})\text{*IPA*IHA} \tag{A1}$$

IF T ≥ GDDTCUT, T = GDDTCUT.
GDD_i accumulated growing degree days at current time step;
GDDBASE base temperature for GDD accumulation (C);
GDDCUT upper temperature for GDD accumulation (C);
T_i air temperature (C);
IPA planting index (1 = on; 0 = off);
IHA harvesting index (1 = off; 0 = on).

$$\mathrm{GDDDAYi} = \mathrm{GDDi}/(\mathrm{Tsec}/\mathrm{DT}) \tag{A2}$$

GDDDAY_i accumulated growing degree days at current day;
T_{sec} total seconds of a day = 24*3600 [s];
DT time step [s];
Crop growth stages determination:

$$\begin{gathered}
\mathrm{JULIAN_i} \le \mathrm{PLTDAY} \Rightarrow \mathrm{PGS} = 1 \\
\mathrm{GDDDAY_i} \ge 0 \Rightarrow \mathrm{PGS} = 2 \\
\mathrm{GDDDAY_i} \ge \mathrm{GDDS1} \Rightarrow \mathrm{PGS} = 3 \\
\mathrm{GDDDAY_i} \ge \mathrm{GDDS2} \Rightarrow \mathrm{PGS} = 4 \\
\mathrm{GDDDAY_i} \ge \mathrm{GDDS3} \Rightarrow \mathrm{PGS} = 5 \\
\mathrm{GDDDAY_i} \ge \mathrm{GDDS4} \Rightarrow \mathrm{PGS} = 6 \\
\mathrm{GDDDAY_i} \ge \mathrm{GDDS5} \Rightarrow \mathrm{PGS} = 7 \\
\mathrm{JULIAN_i} \ge \mathrm{PLTDAY} \Rightarrow \mathrm{PGS} = 8
\end{gathered} \tag{A3}$$

JULIAN_i Julian day of the year;
PGS plant growth stage;
GDDS1 GDD from seeding to emergence;
GDDS2 GDD from seeding to initial vegetative;
GDDS3 GDD from seeding to normal vegetative;
GDDS4 GDD from seeding to initial reproductive;
GDDS5 GDD from seeding to physical maturity.
Carbonhydrate assimilation:

$$\mathrm{CBHYDRAFX} = \mathrm{PSN}\text{*}30\text{*IPA*}(1 - \mathrm{WSTRES})\text{*uca} \tag{A4}$$

CBHYDRAFX carbohydrate assimilated per model step ($\mathrm{g\,m^{-2}}$);
PSN total leaf photosynthesis ($\mu\,\mathrm{mol\,CO_2\,m^{-2}\,s^{-1}}$) (Calculated from Noah-MP);
WSTRES soil water stress (Calculated from Noah-MP);
uca unit conversion factor $a = 10^{-6}$;
ucb unit conversion factor $b = 10^{-3}$.
Maintenance respiration:

$$\begin{gathered}
\mathrm{FNF} = \mathrm{FOLN}/\mathrm{FOLN_MX} \\
\mathrm{TF} = \mathrm{Q10MR}^{**}((\mathrm{TV} - 298.16)/10.) \\
\mathrm{RESP} = \mathrm{LFMR25}\text{*TF*FNF*LAI*}(1. - \mathrm{WSTRES}) \\
\mathrm{RSLEAF} = \mathrm{RESP}\text{*}30\text{*uca} \\
\mathrm{RSROOT} = \mathrm{RTMR25}\text{*}(\mathrm{RTMASS}\text{*ucb})\text{*TF*}30\text{*uca} \\
\mathrm{RSSTEM} = \mathrm{STMR25}\text{*}(\mathrm{STMASS}\text{*ucb})\text{*TF*}30\text{*uca} \\
\mathrm{RSGRAIN} = \mathrm{GRAINMR25}\text{*}(\mathrm{GRAIN}\text{*ucb})\text{*TF*}30\text{*uca}
\end{gathered} \tag{A5}$$

NF foliage nitrogen adjustment to respiration;
TF temperature factor;

TV leaf temperature (K);
Q10MR Q10 for maintenance respiration;
RESP leaf respiration (μmol m^{-2} s^{-1});
FNF foliage nitrogen adjustment to respiration;
FOLN_MX foliage nitrogen concentration (%);
LAI leaf area index;
RSLEAF leaf maintenance respiration per time step (g m^{-2});
RSROOT root maintenance respiration per time step (g m^{-2});
RSSTEM stem maintenance respiration per time step (g m^{-2});
RSGRAIN grain maintenance respiration per time step (g m^{-2});
LFMR25 leaf maintenance respiration at 25°C (μmol co2/kg bio/s);
STMR25 stem maintenance respiration at 25°C (μmol co2/kg bio/s);
RTMR25 root maintenance respiration at 25°C (μmol co2/kg bio/s);
GRAINMR25 grain maintenance respiration at 25°C (μmol co2/kg bio/s);
LFMASS leaf mass (g m^{-2});
RTMASS root mass (g m^{-2});
STMASS stem mass (g m^{-2});
GRAIN grain mass (g m^{-2}).
Growth respiration:

$$\begin{aligned}
&\mathrm{GRLEAF} = \mathrm{FRA_GR}^{*}(\mathrm{LFPT(PGS)}^{*}\mathrm{CBHYDRAFX} - \mathrm{RSLEAF})\\
&\mathrm{GRSTEM} = \mathrm{FRA_GR}^{*}(\mathrm{STPT(PGS)}^{*}\mathrm{CBHYDRAFX} - \mathrm{RSSTEM})\\
&\mathrm{GRROOT} = \mathrm{FRA_GR}^{*}(\mathrm{RTPT(PGS)}^{*}\mathrm{CBHYDRAFX} - \mathrm{RSROOT})\\
&\mathrm{GRGRAIN} = \mathrm{FRA_GR}^{*}(\mathrm{GRAINPT(PGS)}^{*}\mathrm{CBHYDRAFX} - \mathrm{RSGRAIN})
\end{aligned} \tag{A6}$$

GRLEAF growth respiration rate for leaf (g m^{-2} s^{-1});
GRSTEM growth respiration rate for stem (g m^{-2} s^{-1});
GRROOT growth respiration rate for root (g m^{-2} s^{-1});
GRGRAIN growth respiration rate for grain (g m^{-2} s^{-1});
FRA_GR fraction of growth respiration;
LFPT(PGS) fraction of carbohydrate flux to leaf;
STPT(PGS) fraction of carbohydrate flux to stem;
RTPT(PGS) fraction of carbohydrate flux to root;
GRAINPT(PGS) fraction of carbohydrate flux to grain.
Turnover and death:

$$\begin{aligned}
&\mathrm{LFTOVR} = \mathrm{LF_OVRC(PGS)} \quad {}^{*}\mathrm{LFMASS}^{*}\mathrm{uca}\\
&\mathrm{RTTOVR} = \mathrm{RT_OVRC(PGS)} \quad {}^{*}\mathrm{RTMASS}^{*}\mathrm{uca}\\
&\mathrm{STTOVR} = \mathrm{ST_OVRC(PGS)} \quad {}^{*}\mathrm{STMASS}^{*}\mathrm{uca}\\
&\mathrm{SC} = \mathrm{EXP}(-0.3^{*}(\mathrm{TV} - \mathrm{LEFREEZ}))^{*}(\mathrm{LFMASS}/120)\\
&\mathrm{SD} = \mathrm{EXP}((\mathrm{WSTRES} - 1.)^{*}\mathrm{WSTRC})\\
&\mathrm{DIELF} = \mathrm{LFMASS}^{*}\mathrm{uca}^{*}(\mathrm{DILE_FW(PGS)}^{*}\mathrm{SD} + \mathrm{DILE_FC(PGS)}^{*}\mathrm{SC})
\end{aligned} \tag{A7}$$

LFTOVR leaf turnover rate (g m^{-2} s^{-1});
RTTOVR root turnover rate (g m^{-2} s^{-1});
STTOVR stem turnover rate (g m^{-2} s^{-1});
DIELF death of leaf mass rate (g m^{-2} s^{-1});
LF_OVRC(PGS) leaf turnover coefficient (1/s);
RT_OVRC(PGS) root turnover coefficient (1/s);
ST_OVRC(PGS) stem turnover coefficient (1/s);
LEFREEZ characteristic *T* for leaf freezing (K);
DILE_FW(PGS) coefficient for leaf temperature stress death (1/s);

DILE_FC(PGS) coefficient for leaf water stress death (1/s).
Carbohydrate flux allocation:

$$\begin{aligned}
&\text{NPPL} = \text{LFPT(PGS)} \quad \text{*CBHYDRAFX} - \text{GRLEAF} - \text{RSLEAF}\\
&\text{NPPS} = \text{STPT(PGS)} \quad \text{*CBHYDRAFX} - \text{GRSTEM} - \text{RSSTEM}\\
&\text{NPPR} = \text{RTPT(PGS)} \quad \text{*CBHYDRAFX} - \text{RSROOT} - \text{GRROOT}\\
&\text{NPPG} = \text{GRAINPT(PGS)*CBHYDRAFX} - \text{RSGRAIN} - \text{GRGRAIN}\\
&\text{LFMASS} = \text{LFMASS} + (\text{NPPL} - \text{LFTOVR} - \text{DIELF}) \quad \text{*DT}\\
&\text{STMASS} = \text{STMASS} + (\text{NPPS} - \text{STTOVR}) \quad \text{*DT}\\
&\text{RTMASS} = \text{RTMASS} + (\text{NPPR} - \text{RTTOVR}) \quad \text{*DT}\\
&\text{GRAIN} = \text{GRAIN} + \text{NPPG*DT}
\end{aligned} \tag{A8}$$

NPPL leaf net primary productivity ($g\,m^{-2}\,s^{-1}$);
NPPS stem net primary productivity ($g\,m^{-2}\,s^{-1}$);
NPPR root net primary productivity ($g\,m^{-2}\,s^{-1}$);
NPPG root net primary productivity ($g\,m^{-2}\,s^{-1}$).
Convert leaf mass to leaf area index:

$$\text{LAI} = \text{LFMASS *BIO2LAI} \tag{A9}$$

BIO2LAI Leaf area per living leaf biomass (SLA).

Acknowledgments
This project benefitted from the NSF-CAREER-AGS (0847472), USDA-NIFA Agriculture and Food Research Initiative (awards 2011-6800230220, 2015-67003-23508, 2015-67023-23109, 2015-67003-23460, and Hatch 1007699), and NOAA MAPP-CTB grant (NA14OAR4310186). Support for this project was also provided by the Developmental Testbed Center (DTC). The DTC Visitor Program is funded by the National Oceanic and Atmospheric Administration, the National Center for Atmospheric Research, and the National Science Foundation. The simulated data used in this study are available by contacting X. L. (liu744@purdue.edu). The Noah-MP-Crop model is available to download from NCAR-RAL website (https://www.ral.ucar.edu/solutions/products/high-resolution-land-data-assimilation-system-hrldas).

References

Abendroth, L. J., R. W. Elmore, M. J. Boyeer, and S. K. Marlay (2011), *Corn Growth and Development*, *Publ. PMR 1009*, Iowa State Univ. Ext., Ames.
Ball, J. T., I. E. Woodrow, and J. A. Berry (1987), A model predicting stomatal conductance and its contribution to the control of photosynthesis under different environmental conditions, in *Progress in Photosynthesis Research*, vol. IV, pp. 221–224, Martinus-Nijhoff, Dordrecht, Netherlands.
Barlage, M., M. Tewari, F. Chen, G. Miguez-Macho, Z. L. Yang, and G. Y. Niu (2015), The effect of groundwater interaction in North American regional climate simulations with WRF/Noah-MP, *Clim. Change*, *129*, 485–498.
Bonan, G. B. (1996), *Land surface model (LSM version 1.0) for ecological, hydrological, and atmospheric studies: Technical description and users guide. Technical note* (No. PB–97-131494/XAB; NCAR/TN–417-STR), Climate and Global Dynamics Div., National Center for Atmospheric Research, Boulder, Colo.
Bonan, G. B. (2001), Observational evidence for reduction of daily maximum temperature by croplands in the Midwest United States, *J. Clim.*, *14*, 2430–2442.
Cai, X., Z. L. Yang, C. H. David, G. Y. Niu, and M. Rodell (2014), Hydrological evaluation of the Noah-MP land surface model for the Mississippi River Basin, *J. Geophys. Res. Atmos.*, *119*, 23–38, doi:10.1002/2013JD020792.
Changnon, D., M. Sandstrom, and C. Schaffer (2003), Relating changes in agricultural practices to increasing dew points in extreme Chicago heat waves, *Clim. Res.*, *24*, 243–254.
Chen, F., and J. Dudhia (2001), Coupling an advanced land surface-hydrology model with the Penn State-NCAR MM5 modeling system. Part I: Model implementation and sensitivity, *Mon. Weather Rev.*, *129*, 569–585.
Chen, F., and K. Mitchell (1999), Using the GEWEX/ISLSCP forcing data to simulate global soil moisture fields and hydrological cycle for 1987–1988, *J. Meteorol. Soc. Jpn.*, *77*, 167–182.
Chen, F., K. Mitchell, J. Schaake, Y. Xue, H. L. Pan, V. Koren, Q. Y. Duan, M. B. Ek, and A. Betts (1996), Modeling of land surface evaporation by four schemes and comparison with FIFE observations, *J. Geophys. Res.*, *101*, 7251–7268.
Chen, F., et al. (2007), Description and evaluation of the characteristics of the NCAR high-resolution land data assimilation system, *J. Appl. Meteorol. Climatol.*, *46*, 694–713.
Chen, F., et al. (2014), Modeling seasonal snowpack evolution in the complex terrain and forested Colorado Headwaters region: A model intercomparison study, *J. Geophys. Res. Atmos.*, *119*, 13,795–13,819, doi:10.1002/2014JD022167.
Collatz, G. J., J. T. Ball, C. Grivet, and J. A. Berry (1991), Physiological and environmental regulation of stomatal conductance, photosynthesis and transpiration: A model that includes a laminar boundary layer, *Agric. For. Meteorol.*, *54*, 107–136.
Cosgrove, B. A., et al. (2003), Land surface model spin-up behavior in the North American Land Data Assimilation System (NLDAS), *J. Geophys. Res.*, *108*(D22), 8845, doi:10.1029/2002JD003316.
Cowan, I. R., and T. J. Givnish (1986), Economics of carbon fixation in higher plants, in *On the Economy of Plant Form and Function*, pp. 133–170, Cambridge Univ. Press, Cambridge, U. K.
Deryng, D., et al. (2016), Regional disparities in the beneficial effects of rising CO_2 concentrations on crop water productivity, *Nat. Clim. Change*.
Dickinson, R. E. (1983), Land surface processes and climate—Surface albedos and energy balance, *Adv. Geophys.*, *25*, 305–353.
Dickinson, R. E., M. Shaikh, R. Bryant, and L. Graumlich (1998), Interactive canopies for a climate model, *J. Clim.*, *11*, 2823–2836.
Doering, O. C., III, J. C. Randolph, J. Southworth, and R. A. Pfeifer (Eds) (2002), *Effects of Climate Change and Variability on Agricultural Production Systems*, 275pp., Springer, New York.

Ek, M. B., K. E. Mitchell, Y. Lin, E. Rogers, P. Grunmann, V. Koren, G. Gayno, and J. D. Tarpley (2003), Implementation of Noah land surface model advances in the National Centers for Environmental Prediction operational mesoscale Eta model, *J. Geophys. Res.*, *108*(D22), 8851, doi:10.1029/2002JD003296.

Elliott, J., et al. (2015), The global gridded crop model intercomparison: Data and modeling protocols for phase 1 (v1. 0), *Geosci. Model Dev.*, *8*, 261–277.

Freedman, J. M., D. R. Fitzjarrald, K. E. Moore, and R. K. Sakai (2001), Boundary layer clouds and vegetation-atmosphere feedbacks, *J. Clim.*, *14*, 180–197.

Gayler, S., T. Wöhling, M. Grzeschik, J. Ingwersen, H. D. Wizemann, K. Warrach-Sagi, P. Högy, S. Attinger, T. Streck, and V. Wulfmeyer (2014), Incorporating dynamic root growth enhances the performance of Noah-MP at two contrasting winter wheat field sites, *Water Resour. Res.*, *50*, 1337–1356, doi:10.1002/2013WR014634.

Hansen, J. W., and J. W. Jones (2000), Scaling-up crop models for climate variability applications, *Agric. Syst.*, *65*, 43–72.

Harding, K. J., T. E. Twine, and Y. Lu (2015), Effects of dynamic crop growth on the simulated precipitation response to irrigation, *Earth Interact.*, *19*, 1–31.

Hardwick, S. R., R. Toumi, M. Pfeifer, E. C. Turner, R. Nilus, and R. M. Ewers (2015), The relationship between leaf area index and microclimate in tropical forest and oil palm plantation: Forest disturbance drives changes in microclimate, *Agric. For. Meteorol.*, *201*, 187–195.

Jiang, X., G. Y. Niu, and Z. L. Yang (2009), Impacts of vegetation and groundwater dynamics on warm season precipitation over the Central United States, *J. Geophys. Res.*, *114*, D06109, doi:10.1029/2008JD010756.

Jones, J. W., G. Hoogenboom, C. H. Porter, K. J. Boote, W. D. Batchelor, L. A. Hunt, P. W. Wilkens, U. Singh, A. J. Gijsman, and J. T. Ritchie (2003), The DSSAT cropping system model, *Eur. J. Agron.*, *18*, 235–265.

Koster, R. D., and P. C. D. Milly (1997), The interplay between transpiration and runoff formulations in land surface schemes used with atmospheric models, *J. Clim.*, *10*, 1578–1591.

Kumar, A., V. Pandey, A. M. Shekh, and M. Kumar (2008), Growth and yield response of soybean (Glycine max L.) in relation to temperature, photoperiod and sunshine duration at Anand, Gujarat, India, *Am.-Eurasian J. Agron.*, *1*, 45–50.

Levis, S., G. B. Bonan, E. Kluzek, P. E. Thornton, A. Jones, W. J. Sacks, and C. J. Kucharik (2012), Interactive crop management in the Community Earth System Model (CESM1): Seasonal influences on land-atmosphere fluxes, *J. Clim.*, *25*, 4839–4859.

Liu, X., J. Andresen, H. S. Yang, and D. Niyogi (2015), Calibration and validation of the Hybrid-Maize crop model for regional analysis and application over the US Corn Belt, *Earth Interact.*, *19*, 1–16.

Lobell, D. B., G. Bala, and P. B. Duffy (2006), Biogeophysical impacts of cropland management changes on climate, *Geophys. Res. Lett.*, *33*, L06708, doi:10.1029/2005GL025492.

Lu, Y., J. Jin, and L. M. Kueppers (2015), Crop growth and irrigation interact to influence surface fluxes in a regional climate-cropland model (WRF3. 3-CLM4crop), *Clim. Dyn.*, *45*, 3347–3363.

MacKellar, N. C., M. A. Tadross, and B. C. Hewitson (2009), Effects of vegetation map change in MM5 simulations of southern Africa's summer climate, *Int. J. Climatol.*, *29*, 885–898.

McDermid, S., et al. (2015), The AgMIP Coordinated Climate-Crop Modeling Project (C3MP): Methods and protocols, in *Handbook of Climate Change and Agroecosystems: The Agricultural Model Intercomparison and Improvement Project (AgMIP)-Integrated Crop and Economic Assessments*, ICP Series on Climate Change Impacts, Adaptation, and Mitigation, vol. 3, edited by C. Rosenzweig and D. Hille, pp. 191–220, World Scientific, Singapore.

McPherson, R. A., D. J. Stensrud, and K. C. Crawford (2004), The impact of Oklahoma's winter wheat belt on the mesoscale environment, *Mon. Weather Rev.*, *132*, 405–421.

Miller, P., W. Lanier, and S. Brandt (2001), Using growing degree days to predict plant stages, Ag/Ext. Commun. Coord., Commun. Serv., Mont. State Univ., Bozeman.

Neild, R. E., and J. E. Newman (1987), *NCH-40 Growing Season Characteristics and Requirements in the Corn Belt. National Corn Handbook*, Purdue Univ. Cooperative Extension Service, West Lafayette, Ind.

Niu, G. Y., and Z. L. Yang (2004), Effects of vegetation canopy processes on snow surface energy and mass balances, *J. Geophys. Res.*, *109*, D23111, doi:10.1029/2004JD004884.

Niu, G. Y., Z. L. Yang, R. E. Dickinson, L. E. Gulden, and H. Su (2007), Development of a simple groundwater model for use in climate models and evaluation with Gravity Recovery and Climate Experiment data, *J. Geophys. Res.*, *112*, D07103, doi:10.1029/2006JD007522.

Niu, G. Y., et al. (2011), The community Noah land surface model with multiparameterization options (NoahMP): 1. Model description and evaluation with local scale measurements, *J. Geophys. Res.*, *116*, D12109, doi:10.1029/2010JD015139.

Niyogi, D., and J. Andresen (2011), Useful to Usable (U2U): Transforming climate variability and change information for cereal crop producers, Abstract GC13A-0960 paper presented at 2011 Fall Meeting, AGU, San Francisco, Calif.

Niyogi, D., K. Alapaty, S. Raman, and F. Chen (2009), Development and evaluation of a coupled photosynthesis-based gas exchange evapotranspiration model (GEM) for mesoscale weather forecasting applications, *J. Appl. Meteorol. Climatol.*, *48*, 349–368.

Niyogi, D., X. Liu, J. Andresen, Y. Song, A. K. Jain, O. Kellner, E. S. Takle, and O. C. Doering (2015), Crop models capture the impacts of climate variability on corn yield, *Geophys. Res. Lett.*, *42*, 3356–3363, doi:10.1002/2015GL063841.

Oleson, K. W., et al. (2008), Improvements to the Community Land Model and their impact on the hydrological cycle, *J. Geophys. Res.*, *113*, G01021, doi:10.1029/2007JG000563.

Osborne, T., J. Slingo, D. Lawrence, and T. Wheeler (2009), Examining the interaction of growing crops with local climate using a coupled crop-climate model, *J. Clim.*, *22*, 1393–1411.

Pedersen, P. (2004), Soybean growth and development, PM1945, Iowa State Univ. Ext., Ames. [Available at extension.agron.iastate.edu/soybean/documents/Soybeangrowthanddevelopment.pdf (verified 6 Aug. 2015).]

Pielke, R. A., J. O. Adegoke, T. N. Chase, C. H. Marshall, T. Matsui, and D. Niyogi (2007), A new paradigm for assessing the role of agriculture in the climate system and in climate change, *Agric. For. Meteorol.*, *142*, 234–254.

Raddatz, R. L. (1998), Anthropogenic vegetation transformation and the potential for deep convection on the Canadian prairies, *Can. J. Soil Sci.*, *78*, 657–666.

Ramankutty, N., C. Delire, and P. Snyder (2006), Feedbacks between agriculture and climate: An illustration of the potential unintended consequences of human land use activities, *Global Planet. Change*, *54*, 79–93.

Ritchie, S. W., J. J. Hanway, and G. O. Benson (1997), *How a Corn Plants Develops*, *Spec. Publ. 48*, Iowa State Univ. of Sci. and Tech. Coop. and Wheat Spectral Reflectance, Ext. Serv., Ames.

Rosenzweig, C., et al. (2013), The Agricultural Model Intercomparison and Improvement Project (AgMIP): Protocols and pilot studies, *Agric. For. Meteorol.*, *170*, 166–182.

Rosenzweig, C., et al. (2014), Assessing agricultural risks of climate change in the 21st century in a global gridded crop model intercomparison, *Proc. Natl. Acad. Sci. U.S.A.*, *111*, 3268–3273.

Takle, E. S., et al. (2014), Climate forecasts for corn producer decision making, *Earth Interact.*, *18*, 1–8.

Tsvetsinskaya, E. A., L. O. Mearns, and W. E. Easterling (2001), Investigating the effect of seasonal plant growth and development in three-dimensional atmospheric simulations. Part I: Simulation of surface fluxes over the growing season, *J. Clim.*, *14*, 692–709.

Xu, M., and F. Hoffman (2015), Evaluations of CMIP5 simulations over cropland, paper 961003 presented at SPIE Optical Engineering+ Applications, Int. Soc. for Opt. and Photonics, Sept.

Yang, H. S., A. Dobermann, J. L. Lindquist, D. T. Walters, T. J. Arkebauer, and K. G. Cassman (2004), Hybrid-maize—A maize simulation model that combines two crop modeling approaches, *Field Crops Res.*, *87*, 131–154.

Yang, Z. L., and G. Y. Niu (2003), The versatile integrator of surface and atmosphere processes: Part 1. Model description, *Global Planet. Change*, *38*, 175–189.

Yang, Z. L., et al. (2011), The community Noah land surface model with multiparameterization options (Noah-MP): 2. Evaluation over global river basins, *J. Geophys. Res.*, *116*, D12110, doi:10.1029/2010JD015140.